Spatio-temporal analysis of LC3 association to *Mycobacterium tuberculosis* phagosomes in human macrophages

Jacques Augenstreich,[a#] Anna T. Phan,[a] Charles N.S. Allen,[a] Lalitha Srinivasan,[a,b] Volker Briken[a#]

[a] Department of Cell Biology and Molecular Genetics, University of Maryland, College Park, USA
[b] Current address : Meso Scale Discovery, Rockville, MD, USA
[#] Correspondance : jaugenst@umd.edu ; vbriken@umd.edu

Abstract

Autophagy can act as a defense mechanism for macrophages infected by intracellular pathogens. *Mycobacterium tuberculosis* (Mtb) is known to both induce and repress autophagic responses, such as xenophagy and LC3-associated phagocytosis (LAP) which both involve the recruitment of LC3 to the Mtb-containing vacuole (MCV). However, the dynamics of MCV interaction with xenophagy or LAP are unclear. Here, using time-lapse confocal microscopy, we present a comprehensive spatio-temporal analysis of the LC3 recruitment to the MCVs during the infection of macrophages. The results revealed frequent LC3 recruitment in the form of large tubule-vesicular structures to the MCV, characteristic of xenophagy, and demonstrated that Mtb could efficiently escape from this signal. We found that the main driver of the LC3 recruitment is the initial macrophage bacterial burden before a second phagocytosis event. We also assessed the potential bactericidal properties of the LC3 recruitment and observed that interferon-gamma treatments did not affect the LC3 recruitment frequency. Additionally, no sign of acidification in the formed autophagosome with or without interferon-gamma treatment was observed. Interestingly, the time-lapses using the acidification probe lysoview revealed that the LC3 recruitment happened shortly after a drop in acidity, a typical sign of membrane damage that is a well-known trigger for autophagy. However, LC3 subsequent loss of signal or escape could also be followed by a restoration of acidification in the vacuole, thus showing restoration of membrane integrity. In conclusion, we show that LC3 recruitment to the MCV correlates with subsequent membrane repair. However, the LC3 recruitment did not show bactericidal properties, questioning its cell intrinsic role in controlling the Mtb infection in macrophages.

Introduction

Mycobacterium tuberculosis (Mtb) is the causative agent of the pulmonary disease tuberculosis, which is one of the deadliest bacterial infections worldwide (WHO). The primary niche of replication for Mtb during infection is the macrophage.[1–4] An important characteristic of intracellular Mtb is its ability to evade host cell microbicidal responses.[5–7] One mechanism of the cell-intrinsic host defense is targeting phagocytosed bacteria by host cell autophagy to create an autophagosome through a process called xenophagy.[8] An important marker for autophagy activation is the protein Microtubule-associated proteins 1A/1B light chain 3B (LC3), which is recruited to the membrane of the forming phagophore for the final formation of the autophagosome.[8] The recruitment of LC3 to phagosomes can also happen independently of the canonical autophagic machinery in a process called LC3-associated phagocytosis (LAP). Xenophagy limits Mtb proliferation in mouse macrophages,[9,10] but it seemed overall inefficient in controlling Mtb growth in human macrophages,[11] despite the activation of xenophagy signaling.[10,12–14] LAP also has a protective role in murine macrophages, but its capacity to inhibit Mtb replication in human macrophages has not been clearly demonstrated.

Even though they are related to the autophagic machinery, xenophagy and LAP are triggered in very distinct ways. During Mtb infections, xenophagy is mainly induced by membrane damage induction, which allows the recruitment of galectin proteins that recruit proteins of the autophagic machinery[9,15–18]. In contrast, LAP is independent of membrane damage induction and relies on TLR signaling[19], and LC3 recruitment to the phagosome is dependent on the production of reactive oxygen species (ROS) by the NOX2 complex[20]. Ultimately, both LAP and xenophagy activation is followed by phagosome/autophagosome maturation[21]. This maturation occurs even though LC3 and autophagic machinery proteins were found to be dispensable for phagosome maturation characterized by acidification or LAMP1 recruitment.[22]

Mtb infection leads to the activation of autophagy signaling, but bacteria can inhibit steps of xenophagy and LAP to increase their survival within macrophages.[14] In the model system of *Dictyostelium discoideum* infected by *Mycobacterium marinum* (Mma), the phagosome escape by Mma triggers xenophagy, but the maturation of the autophagosome is blocked by the bacteria.[23,24] This inhibition of the maturation of the autophagosome was also observed in Mtb-infected human dendritic cells[25] and macrophages.[26] The inhibition of the maturation of the autophagosome is, at least partially, mediated by the Mtb cell envelope lipid phthiocerol dimycocerosate (DIM/PDIM).[14] The Eis and PE-PGRS47 proteins are among several Mtb proteins that have been identified to mediate the inhibition of host cell xenophagy (for review[6]).[27–30] The spatio-temporal analysis of xenophagy via live cell imaging highlighted that Mtb could escape from the newly formed autophagosome.[12] Mtb inhibited LAP via CpsA; however, the inhibition of LC3 recruitment was overcome by treating the macrophages with interferon-Gamma (IFN-γ).[31]

The crosstalk between Mtb and LC3-dependent responses (*i.e* xenophagy, LAP) is highly dynamic and shows a duality between induction and inhibition of these responses by the bacteria. Autophagy signaling has been proposed as a potential host-directed therapy target for Mtb infections.[32] But the fact that Mtb can, at least temporarily reside and survive in autophagosomes[12] which are considered a bactericidal environment, raises the question of how efficient these LC3-

driven host responses are in controlling Mtb replication. In this study, we monitored the dynamics of LC3 association to the phagosome during the infection of THP-1 cells with Mtb using time lapse confocal microscopy. We also developed a new analysis workflow combining different methods of deep learning-based segmentation and rational tracking of cells to analyze fluorescence signals at the single-cell level. The results show that about 70% of mycobacteria-containing vacuoles (MCVs) become positive for LC3 at least once during recording, with about 40% of these MCVs that can escape initial LC3 recruitment. We demonstrate that there is a wide range of times post infection that the MCV recruits LC3 and that the time of recruitment is independent of the number of bacteria per MCV showing a lack of coordinated response from autophagy. Instead, additional Mtb phagocytosis in an already infected cell seems to trigger LC3 recruitment on all MCVs. Next, we investigated how bactericidal these responses were and we observed that the priming of cells with IFNγ does not affect LC3 recruitment nor acidification of the MCV. However, in most cases LC3 recruitment was preceded by acidification of the MCV followed by a drop when LC3 is recruited. We also observed that in some cases we found a recovery of acidification associated with a loss of LC3 signal, showing a repair of the phagosome membrane.

Results

The majority of MCVs undergo LC3 recruitment during infection

Multiple studies have shown that Mtb can induce autophagy at specific time points post-infection. Autophagy was evaluated by immunofluorescence staining on fixed samples[14,16] or stable expressions of recombinant fluorescence proteins,[12,13] but for the latter lacked clear quantification and timing determination. Consequently, these studies offered an incomplete view of the dynamic events and, for example, did not allow to determine if LC3 recruitment to the MCV follows a specific timing after phagocytosis.

To evaluate the LC3-associated responses during infection with Mtb, we used PMA-differentiated THP-1 cells stably expressing LC3-GFP[33] and infected them with a fluorescent strain of Mtb (H37Rv-DsRed). The cells were followed by time-lapse confocal microscopy during 16-20 hours after the addition of bacteria at on MOI of 2 (Figure 1A, Movie 1). The LC3 recruitment to the MCV was monitored from the time of phagocytosis to the end of recording for individual MCV. Results showed that ~70% of MCVs triggered LC3 recruitment (Figure 1B) at one point or another after phagocytosis. However, almost half of the LC3-positive ($LC3^+$) MCVs became negative by the end of the recording showing efficient escape of Mtb from the LC3 recruitment. We also observed two patterns of escape from LC3 recruitment by Mtb (Figure 1C-D). One pattern (Exclusion) which is characterized by an initial increase of the LC3 signal at the MCV that quickly diffused away from the bacteria (Figure 1C, Movie 2). The other pattern observed (Egress) is characterized by the accumulation of LC3 signal at the MCV with the formation of tubulovesicular structures (TVS),[34] then the bacteria and the TVS separate (Figure 1D, movie 3). An example of continuous recruitment of LC3 to the MCV is shown with the formation of an Mtb-containing autophagosome (Figure 1E, Movie 4). Overall, LC3 recruitment seemed frequent around MCVs

(~70% of all observed MCVs), but in a significant fraction of these recruitments (about 40%) the bacteria appear to escape from the response.

No correlation between autophagy induction and the time after infection nor the size of the MCV

Given the dynamic nature of LC3-MCV interactions (Figure 1) we deepened the analysis of LC3 recruitment to MCVs. We analyzed a total of 73 MCVs showing at least one temporary LC3 recruitment by their time post-phagocytosis and their observed length of time of LC3 recruitment (table 1). Three groups of MCVs could eventually be distinguished: (i) MCVs showing LC3 recruitment between 0 and 1 h post phagocytosis (hpp) (Table 1, Figure 2B, C), (ii) MCVs showing recruitment after 1 hpp and (iii) the MCVs presenting multiple LC3 recruitment events. For each group, an example is given (Figure 2B–G), where the fluorescence quantification on the bacterial area over time (Figure 2C,E,F, Movies 4-6) could confirm the visual observation as shown on representative snapshots from the time-lapse study (Figure 2B,D,F). We observed a 40 minutes gap between early and late recruitment events, meaning that in the early event category LC3 recruitment was always observed between 0 to 0.33 hpp and the recruitment in the late event category started after 1 hpp (Table 1). However, within the late events group no clear pattern emerged that would indicate that the LC3 recruitment is governed by a clear timing factor. Instead, we observed a wide range of LC3 recruitment times, from 1 to about 13 hpp. indicating an absence of a coordinate response involving LC3 after Mtb phagocytosis.

In summary, LC3 recruitment to MCVs is highly variable in timing, from early recruitments (< 0.33 hpp) to late recruitments (> 1 hpp), without clear patterns of a coordinated response.

A previous study proposed that the number of bacteria per MCV and more specifically their capacity to form cords could inhibit xenophagy.[35] Intracellular cord formation is not occurring in differentiated THP-1 cells and thus could not be a factor in our system but the influence of bacterial burden per cell on LC3-recruitment could be assessed. First, we compared the number of bacteria per MCVs to the time post infection when the first LC3 recruitment was observed (Figure 3A). A slight trend might be observed where the more bacteria per MCVs, the faster the LC3 recruitment seemed to be, but it failed to show any statistical correlation (R^2= 0.072). This was confirmed by analyzing the average number of bacteria per MCV among the groups described in Table 1. On average, the number of bacteria per MCV was not different between the early and late recruitment groups or the group with multiple recruitment events (Figure 3B).

Initial bacterial burden is the main driver of LC3 recruitment.

Even though the size of the MCV itself did not appear to correlate with initiation of LC3 recruitment, in some infected cells, it seemed that subsequent LC3 recruitment happened because other MCVs were already present inside the cell. For example, in this recording of the cells (Figure 1D, Movie 3), the first bacteria entered the cell, and no LC3 recruitment to the MCV was observed

for 11 hours and 50 minutes. Then a second bacterium was phagocytosed and immediately (≤ 10 min) triggered LC3 recruitment to that MCV. Interestingly, in this cell even the first MCV underwent LC3 recruitment shortly after the second MCV became $LC3^+$. This series of events suggested that the second MCV triggered a response that then targeted both MCVs.

To analyze this phenomenon on a larger number of single cells, we optimized a new analysis method that combines multiple existing methods (see *methods*, Figure S1). With a lack of phase contrast or differential interference contrast microscopy images, to efficiently segment cells, we used deep learning-based segmentation from the Cellpose 2.0 software.[36] This approach successfully segmented cells even in groups of 5 to 7 touching cells (Figure S1). The tracking of cells based on the segmentation was done according to another study on tracking Mtb bacterial burden in infected macrophages.[3] The combination of these methods allowed for the successful tracking of single cells and the collection of quantitative data over the time lapses. Infected cells that presented LC3 recruitment to MCVs were selected (Figure 3C, movie 8). Integrated LC3 was plotted against integrated DsRed fluorescence (Figure 3D). Results showed a clear correlation between increased LC3 signal and increased DsRed signal. A color code was also applied for time as a 3rd dimension, and it confirmed the results in Table 1 that the timing factor does not seem to correlate with the increased LC3 signal. We also plotted the DsRed signal over time with a color variation for LC3 recruitment (Figure 3E). This representation confirmed the correlation between LC3 and bacterial signals and indicated that a higher LC3-associated response was observed with higher bacterial loads. In summary, the results showed that the bacterial burden of macrophages rather than the size of the MCV was directly associated with LC3 recruitment.

$LC3^+$ MCVs do not acidify, and their frequency is not affected by IFN-γ pre-treatment of macrophages.

During the time-lapses, a non-negligible number of bacteria did not show signs of escaping LC3 association (Figure 1B) suggesting that they might be contained in autophagosomes that could mature and eventually kill the bacteria. To explore the fate of $LC3^+$ MCVs, the cells were infected for 4h and later dyed with Lysotracker blue (LTB) to assess phagosome or autophagosome acidity (Figure 4A). Strikingly, at 16 hours post-infection, none of the $LC3^+$ MCVs were positive for LTB, although about 15% of MCVs were positive for LTB (Figure 4B). These results strongly suggested that LC3 recruitment does not result in Mtb contained within autophagolysosomes. Previous studies showed that pretreatment with IFN-γ increased LC3 association with MCVs and phagosome maturation.[4,31] To study this in a live-imaging condition, we opted for the far-red probe Lysoview-633 (LV), which showed a similar pattern to LTB at 24 hours post-infection and was not cytotoxic when left in the medium for 48 hours (Figure S2). The result of the pretreatment of THP-1-LC3-GFP cells with 10 ng/mL of IFN-γ overnight showed that the pretreatment did not affect the LC3 association level to MCVs and did not increase the phagosome maturation level at 6 hours post-infection, nor did it increase the number of acidified $LC3^+$ MCVs (Figures 4D). However, pretreatment with IFN-γ made the cells more susceptible to Mtb-induced cell death, characterized by "ballooning" morphology as observed through the transmitted light channel (Figure 4C, movie 9, 10). The quantification of this phenomenon at 20 hours post-infection showed

an increase from 40% in untreated cells to 75% in IFN-γ pretreated cells after Mtb infection (Figure 4E). In summary, our results showed that LC3 recruitment almost never turned into a mature autophagolysosome, and that IFN-γ was not able to increase the frequency of LC3 recruitment or the maturation level of the autophagosomes.

LC3 recruitment to and acidification of the MCVs are mutually exclusive events.

Our steady state analysis showed minimal percentage of MCVs that were positive for LC3 and lysotracker staining (Figure 4B). From the untreated cells in figure 4C-E, we selected MCVs that showed LC3 recruitment and could be followed for at least 3h to investigate the dynamics of LV and LC3 association with the MCV. The analysis showed that LC3 and LV staining does not happen simultaneously (Figures 5A–D, Figure S4). Instead, we observed acidification of the MCV, followed by a drop of acidification prior to the subsequent LC3 recruitment. In some cases, the LC3 signal dropped and was followed by a quick recovery in acidification thus completing a cycle that could be repeated (Figures 5A, B, Movie 11). In other cases, the LC3 recruitment would persist for prolonged periods of time (>6h) until the end of the recording (Figures 5C, D, Movie 12). We did not observe cased in which the MCVs became $LC3^+$ without first acidifying ($LV^{+)}$. We also did not observe cases in which the LV^+ MCVs lost acidification without gaining LC3 staining. To further visualize the link between acidification and LC3 recruitment, we plotted the LC3 signal from single MCVs against the LV fluorescence at every time point recorded (Figure 5E). The resulting dot plot and density map clearly show two populations of stained MCVs, the $LC3^+$ ones, and the LV^+ ones with very rare amount of double positive MCVs. This result confirms the observation that $LC3^+$ phagosomes are rarely acidic and that an acidified vacuole loses its acidification before LC3 recruitment, indicating that membrane damages occurred and were recognized by the autophagic machinery. The eventual recovery of acidification after LC3 loss of signal was also suggesting membrane repair involving the autophagy machinery.

Discussion

Mtb manipulates many host cell signaling pathways in order to survive and replicate in macrophages.[6,7] A hallmark discovery was the observation that Mtb inhibits the maturation process of the MCV.[37] Many additional reports established a dogma that Mtb remains within an immature phagosome during its intracellular infection phase.[38–42] This dogma was overturned when it was shown that a fraction of the bacteria can escape the MCV into the cytosol.[43,44] Additional studies show that a fraction of MCVs do not inhibit phagosome maturation but acidify and obtain characteristics of phagolysosomes.[43,45] It is not uncommon for intracellular bacterial pathogens to occupy several intracellular niches.[46] What is the interaction of these different populations of bacteria within the infected cell and how does the niche that Mtb occupies determine its interaction with the host cell autophagy machinery? For example, the contact of the bacteria with the cytosol triggers ubiquitination of Mtb involving the E3 ligase Parkin and the DNA sensor STING, that can

trigger xenophagy in an attempt to recapture the bacteria.[9,17] To start answering these questions we performed spatiotemporal analysis of the interaction of individual bacteria with the host cell LC3 protein as a marker for autophagy responses.

The results of our study and of previous published data are summarized in the model shown in Figure 6 which focuses on the MCV and the observed role of LC3 recruitment. A novel finding is that the process of acidification of the MCV was observed preceding membrane damage-induced loss of acidification and subsequent recruitment of LC3 (Figure 6). At this point at least two options are possible: 1) the MCV loses LC3 and re-acidifies and another cycle of LC3 recruitment could occur or 2) the LC3 recruitment persists. A previous study using correlative light electron microscopy (CLEM) approaches in Mtb-infected human monocyte-derived macrophages and iPSCDM shows that the vast majority of intracellular Mtb do not enter autophagosomes since they are not contained within the characteristic double membrane compartments.[12] Mtb can either escape the autophagosome, or it was proposed that it could induce a local autophagic response away from the MCV or the cytosolic bacteria.[12] In our study these $LC3^+$ MCVs do not acidify (Figure 4,5) which shows that the bacteria are still in a favorable environment since low pH of $LC3^+$ autophagosomes is a marker of autolysosome generation which is typically associated with a bactericidal host response. We did not observe the scenario in which an $LC3^+$ MCV loses LC3 staining but did not acidify (Figure 5). This could have been interpreted as becoming an MCV that has the characteristics of an immature phagosome or that the bacteria escaped into the cytosol (Figure 6).

LC3 recruitment to the MCV is dependent upon the Mtb ESX-1 secretion system and requires damage to the phagosome membrane since galectin-8 recruitment precedes LC3 recruitment to the MCV.[5,12,15] We observed that acidification is frequently observed before we can observe LC3 recruitment (Figure 5). This acidification was suggested as a trigger for Mtb to induce membrane damages. Indeed, the Mtb transcriptional regulator PhoP/R system seems to be activated by slightly acidic pH[47] and PhoP/R is a positive regulator of EsxA secretion.[48] In addition, the membrane lytic activity of EsxA is increased by an acidic pH potentially via the pH-mediated dissociation of EsxA from its chaperon EsxB.[49–51] Hence the acidification of the MCV we observe could lead to increased levels of active EsxA within the phagosomal lumen which results in phagosomal membrane damage. However, it was also shown that phagosome maturation blockade was a prerequisite for Mtb phagosome escape[52] and that phagosome acidification with bafilomycin could strongly promote phagosome membrane damages.[52,53] Accordingly, in our study data set, many bacteria did not show signs of escape from acidification and persisted in this environment for the whole recording. Thus, the requirement of acidification to induces membrane damages is still an open question. Additionally, the lysoview probe documentation indicates it could emit fluorescence at $pH \leq 7$. It was proposed that the phagosome maturation blockade by Mtb stabilize the pH at ~ 6.5, which could still potentially be stained by lysoview in our experimental conditions. Thus, we cannot differentiate highly acidic compartments to the phagosome where Mtb at least partially blockaded the maturation and consequently additional studies would be required to conclude on the matter.

We did not include membrane damage markers such as galectin-3 or 8 into our study but the loss of acidity as reported by the loss of lysotracker/lysoview staining is an indicator of membrane damage since it was initially used to follow lysosome damage and repair mechanisms via live cell imaging.[54–57] Importantly, this method has been used to assess phagosomal membrane damage during Mtb infections as well.[12,58] Thus, it is reasonable to conclude that this loss of acidification shows induction of phagosomal membrane damage by Mtb. The time-lapse analysis shows that acidic MCV lose lysoview staining right before they recruit LC3 (Figure 5). The rapid and subsequent LC3 recruitment observed here has also been previously associated with membrane damage.[12,13,15,16] This observation is also in agreement with the role of LC3 in phagosome membrane repair during Salmonella infections[59] and a similar proposed mechanism during *Mycobacterium marinum* infections.[23,24] In conclusion, our observations can be explained by the EsxA-induced phagosomal membrane damage, leading to loss of acidity and recruitment of autophagy related membrane repair machinery. How exactly the formed autophagosome or TVS act as a repair mechanism is still to be determined. An hypothesis could be that the autophagosome could serve as a membrane material source, similar to the lysosome membrane repair mechanism involving the endoplasmic reticulum.[57]

Our study failed to observe signs of LAP being induced after Mtb phagocytosis as the events of LC3 recruitment showed tubulovesicular structure formation, which is induced during canonical autophagy or xenophagy and is distinctively different from LC3 lipidation at the phagosome membrane.[60] Also, we did not detect MCVs that were acidified and $LC3^+$ and a recent study found that LAP was dependent on V-ATPase recruitment to the phagosome and that the stabilization of the complex by saliphenylhalamide further stimulated the LAP and LC3 recruitment.[61] We can propose a hypothesis for the lack of detection of LAP in our work. First, Mtb inhibits LAP through the NOX2-inhibiting activity of the Mtb CspA protein[31] and this inhibition might be more potent in human macrophages when compared with BMDMs, in which most of the published work has been performed to date. Another explanation could be the dependency of ROS production for triggering LAP. Indeed, Mtb possesses multiple factors that can neutralize the ROS produced, like KatG[62] and SodA,[63] and other factors linked to a decrease in ROS production, such as NuoG.[64] Another study also found that PPE2 can bind p67, a subunit of the NOX-2 complex, to prevent ROS production.[65] In summary, all these factors could prevent LAP and the associated LC3 recruitment. Hence, we think that the LC3 recruitment to the MCV in our study was almost exclusively associated with an autophagy-related membrane damage repair mechanism and/or autophagosome formation.

Our experimental approach allowed us to determine at what time after phagocytosis MCVs become $LC3^+$ and we noticed that there was a wide range of times post-infection that this event could occur (table 1). Thus, we investigated if LC3 recruitment could be linked to the number of bacteria per MCV by tracking the bacterial fluorescence signal per MCV and the LC3-GFP signal over time. Our results showed that there was no correlation between the number of bacteria per MCV and the time of LC3 recruitment (Figure 3A). Quantification of the average number of bacteria per MCV exhibiting early recruitment (< 1 hour) or late recruitment (> 1 hour) also demonstrated no difference (Figure 3B). To the best of our knowledge this is the first time that a detailed analysis and quantification of these parameters was done since the only other time-lapse study following

LC3 recruitment onto MCVs aimed to study the structure of $LC3^+$ MCV by CLEM and FIB-SEM imaging[12]. We made the observation that an MCV failed to show LC3 recruitment for 10 hours but became $LC3^+$ soon after another bacteria was phagocytosed into the same cell. So, we hypothesized that the existence of an MCV prior to the phagocytosis of a new bacterium could triggers LC3 recruitment to all MCVs. To test the hypothesis, we optimized a new workflow to analyze the correlation between the fluorescence of LC3-GFP and Mtb-DsRed at the single-cell level over time. Our method combined existing protocols of cell segmentation by deep learning using the Cellpose software[36] and another cell tracking protocol that was used in this study[3] to collect quantitative data; however, this tracking protocol relied on MATLAB. In our study, the tracking was implemented from open-access software, excel and ImageJ. The use of deep learning-based segmentation allowed for the successful recognition of individual cells within groups containing multiple touching cells in our dataset. Our method was an important improvement as typical cell detection usually exploits phase contrast microscopy images,[66,67] which were unavailable in our microscopy configuration, and the edge detection was not optimal for the segmentation of touching cells.

Applying this workflow to our time-lapse data, we were able to select single cells that got infected and show that LC3 recruitment was strongly correlated with the overall bacterial burden of the cells. This approach quantifies the second or potentially third phagocytosis event per cell due to the increase in Mtb-DsRed staining. Theoretically, the replication of Mtb within a single MCV could also increase the total fluorescence of the cell thus confounding it with additional phagocytosis events. We do not think that this affects the results because we limited the time post-infection to 20 h which is below the usual Mtb double time of about 24 h and secondly, Mtb seems to replicate mostly in necrotic cells which were not included in our analysis.[3,4] The interesting question now is how the initial phagocytosis affects the LC3-recruitment response of a secondary phagocytic event? The primary phagocytosis event triggers hosts cell signaling cascades which may led to an activation status that affect how the host cell response to a second phagocytosis event. A not mutually exclusive pathway could be that the second MCV pushes the autophagy-related membrane machinery above an activation threshold by increasing the amount of damaged membranes in the cell.

The final aspect of this LC3 recruitment study was to investigate how potentially bactericidal the LC3 recruitment could be by looking at the acidification level of the phagosome/autophagosome and at IFN-γ stimulation that is supposed to enhance the phagosome/autophagosome maturation.[31] In contrast to other studies in BMDMs,[31] IFN-γ pretreatment did not affect LC3 recruitment and phagosome acidity at 6 hours post-phagocytosis. This results shows a potentially crucial difference between mouse and human macrophages and confirms what was reported elsewhere that IFN-γ had no noticeable effect on Mtb fitness in primary human macrophages[4,12] and phagosome maturation.[4] However, in our study, IFN-γ had a strong effect on macrophage viability during infection. This unexpected result might be caused by a similar cell death mechanism observed in macrophages stimulated with LPS and IFN-γ, which was able to cause a necrotic type of cell death which is not associated with a protective host response to Mtb infections.[68]

In conclusion, autophagy pathways are widely described as potential targets for host-directed therapy since the induction of autophagy has been described to control Mtb growth in macrophages. However, there is growing evidence that while this might be the case in mouse macrophages, autophagy seems inefficient at controlling Mtb in human macrophages.[12] Consistently, our study shows that although autophagy is frequently induced during infection of human macrophages with Mtb due to membrane damage induction, the bacteria are able to either evade xenophagy by escaping the forming autophagosome or block the bactericidal effects of xenophagy by inhibiting the maturation of the autophagosomes.

Material and methods

Reagents and antibodies

Lysotracker blue (Molecular Probes), Lysoview-633 (biotium), Phorbol-Myristate-Acetate (PMA, provider), RPMI medium (Gibco), Fetal Bovine Serum (FBS, Gibco), DPBS 1X (Gibco), Recombinant human Interferon Gamma (R&D Systems), OADC supplement (R&D Systems), Zeocin (invivogen).

Mycobacterial strain and culture

The DsRed-expressing strain of *M. tuberculosis* H37Rv was generated by cloning the *dsred* gene from the pMSP12-dsred2 (addgene #30171) into pMAN-1 expression vector previously used[69] by EcoRI and HindIII digestion. The *dsred* gene was amplified using the following primers sequences:

Forward CGGCGAATTCATGGCCTCCTCCGAGAACG;

Reverse GGCTAAGCTTCTACAGGAACAGGTGGTGG

Bacteria were grown in liquid Middlebrook 7H9 medium supplemented with 10% oleic acid-albumin-dextrose catalase (OADC) growth supplement, 0.2% glycerol, 0.05% tween 80, and Zeocin 100µg/mL. For infections, the bacteria were washed in 0.05% PBS-tween 80 before being added to the infection medium (see procedure below).

Monocyte culture, differenciation and infection

GFP-tagged LC3 expressing THP1 monocytes (THP-1-LC3-GFP) were provided by Dr. John Kehrl (NIH) and used in a previous study.[33] The cells were cultured in RPMI 1640 (ATCC modification) supplemented with 10% heat-inactivated Fetal bovine serum (complete medium). The cells were differentiated with 20 ng/ml of PMA for 20–24 hours. In the case of IFN-γ pre-stimulation, the cells were washed in 1X DPBS and incubated overnight with 10 ng/mL of IFN-γ in complete medium. Stimulation efficiency was evaluated by flow cytometry and by the staining of MHC-II (HLA/DR) surface expression (Figure S3).

For infections, cells were washed in 1X DPBS and incubated in RPMI supplement with 5% normal human AB serum (infection medium). The bacteria were added to the cell at an MOI of 2 without a washing step for time-lapse imaging or an MOI 10 for 4 hours for single time point imaging. After the 4-hour incubation, cells were washed and incubated for 16 hours in complete medium supplemented with 100 µg/mL Gentamycin.

Time-lapse confocal microscopy

THP-1 cells were seeded and differentiated in glass-bottom observation chambers (ibidi) at $2x10^5$ cells/well. The cells were stimulated with IFN-γ, if needed, before the infection (see above). For imaging of phagosome maturation, the infection medium was supplemented with Lysoview-633 at a final concentration of 1:2000 in infection medium and left on the cells during recording. The cells were imaged using a Zeiss laser scanning confocal microscope LSM-800, equipped with two gallium arsenide phosphide photomultiplier tube (GaAsP-PMT) detectors and a transmitted light photomultiplier tube detector (T-PMT), using the 63x/NA1.4 Oil objective. The observation chamber was maintained at 37°C and supplied with 5% CO2 through a humidifier system. A 10 µm z-stack (1 µm steps) was acquired every 10 minutes on 4 to 8 fields of view over 16 to 20 hours.

To assess phagosome maturation using lysotracker blue, the cells were infected in glass bottom observation chambers at an MOI of 10, as described above, and incubated for 16 hours. The cells were washed three times with 1X DPBS and incubated in complete medium supplemented with 1:10000 lysotracker blue for 30 minutes. The cells were washed, incubated in complete culture medium, and imaged by confocal microscopy.

Image analysis and single cells tracking

All the MCV qualitative assessments of LC3 recruitment, fluorescence quantifications, and single MCV tracking were performed using the ImageJ/Fiji software using custom macros. The method for quantifying the fluorescence at the MCV over time was previously described.[70]

Figure 3 shows the implemented new analysis workflow combining the existing methods and software. A simplified diagram is shown in Figure S1. The first step consisted of segmenting the cells from the transmitted light (T-PMT) channel. Specifically, the first or second slice of the time lapses stacks were extracted using the "make substack" function in Fiji. The created time-lapse was decomposed into single frames and saved in a dedicated folder. Secondly, we used the deep-learning segmentation software Cellpose. We trained the "Livecells" model using our data set, specifically by randomly picking frames from the performed experiments. The trained model was then used to segment the rest of the frames from every time lapse. From the segmentation mask generated, movies were reconstructed on ImageJ using the "concatenate" tool. The mask time lapses were then used to generate regions of interest (ROIs) around the cells on each frame, allowing us to collect the x and y coordinates of the ROIs. These ROIs were also applied to the summed z-projection of the corresponding time lapses to collect the total normalized fluorescence intensity (IntDen) of LC3-GFP and the Raw total fluorescence intensity (RawIntDen) of DsRed from the bacteria. However, although this approach allowed the collection of a large amount of data, each data point only corresponded to one cell in one time frame. The cells in each frame and the same field of view were linked to cells in the previous frame by the root mean squared closest centroid, using the equation:

$$Dist = \sqrt{|(x_i - x_{i+1})|^2 + |(y_i - y_{i+1})|^2}$$

Where x_i and y_i are one ROI coordinates of frame i. x_{i+1} and y_{i+1} are ROI coordinates in frame i + 1. The calculation is reiterated between one ROI and all of the ROI in the next frame, and the

minimal distance value was retained. This allowed us to recreate the ROI and corresponding fluorescence traces obtained earlier. All the calculations and ROI linking were performed using excel, and the ROI traces were manually curated using ImageJ.

Data representation and statistics

Data were plotted using Graphpad Prism 9 except for the density map in Figure 5E, which was created using R. The figures were designed using Powerpoint and Inkscape, and the model design was made using Inkscape. All statistical tests were performed using Prism. The correlation between two variables was tested using Pearson's correlation test. Statistical differences between two groups were tested using unpaired Student *t*-tests or more than two groups using a one-way ANOVA followed by Dunnett *post-hoc* statistical test. Comparisons with a *p*-value greater than 0.05 were considered significant.

Data and code availability

All data, code used for macros, and calculations are available from the corresponding authors upon reasonable requests.

Acknowledgements

We thank Adrien Schahl for his insights in the optimization of the cell tracking calculation.

This work was supported by the National Institute of Allergy and Infectious Diseases (Grant R01AI139492 to V.B.)

V.B and J.A. designed the experiments and wrote the manuscript. V.B., J.A., C.N.S.A., and A.T.P., edited and proofread the manuscript. J.A. and A.T.P. performed the experiments. J.A., A.T.P., C.N.S.A. analyzed the results. J.A. and C.N.S.A. developed the single cells tracking tool used in this study. L.S. created the fluorescent Mtb strain.

We declare no conflicts of interests

References

1. Davis, J. M. & Ramakrishnan, L. The Role of the Granuloma in Expansion and Dissemination of Early Tuberculous Infection. *Cell* **136**, 37–49 (2009).
2. Cohen, S. B. *et al.* Alveolar Macrophages Provide an Early Mycobacterium tuberculosis Niche and Initiate Dissemination. *Cell Host Microbe* **24**, 439-446.e4 (2018).
3. Mahamed, D. *et al.* Intracellular growth of Mycobacterium tuberculosis after macrophage cell death leads to serial killing of host cells. *eLife* **6**, e22028 (2017).
4. Lerner, T. R. *et al.* Mycobacterium tuberculosis replicates within necrotic human macrophages. *J. Cell Biol.* **216**, 583–594 (2017).
5. Queval, C. J., Brosch, R. & Simeone, R. The Macrophage: A Disputed Fortress in the Battle against Mycobacterium tuberculosis. *Front. Microbiol.* **8**, 2284 (2017).
6. Augenstreich, J. & Briken, V. Host Cell Targets of Released Lipid and Secreted Protein Effectors of Mycobacterium tuberculosis. *Front. Cell. Infect. Microbiol.* **10**, (2020).
7. Chandra, P., Grigsby, S. J. & Philips, J. A. Immune evasion and provocation by Mycobacterium tuberculosis. *Nat. Rev. Microbiol.* 1–17 (2022) doi:10.1038/s41579-022-00763-4.
8. Deretic, V. Autophagy in inflammation, infection, and immunometabolism. *Immunity* **54**, 437–453 (2021).
9. Manzanillo, P. S. *et al.* The ubiquitin ligase parkin mediates resistance to intracellular pathogens. *Nature* **501**, 512–516 (2013).
10. Gutierrez, M. G. *et al.* Autophagy Is a Defense Mechanism Inhibiting BCG and Mycobacterium tuberculosis Survival in Infected Macrophages. *Cell* **119**, 753–766 (2004).
11. Andersson, A.-M. *et al.* Autophagy induction targeting mTORC1 enhances Mycobacterium tuberculosis replication in HIV co-infected human macrophages. *Sci. Rep.* **6**, 28171 (2016).

12. Bernard, E. M. *et al.* M. tuberculosis infection of human iPSC-derived macrophages reveals complex membrane dynamics during xenophagy evasion. *J. Cell Sci.* **134**, jcs252973 (2020).
13. Beckwith, K. S. *et al.* Plasma membrane damage causes NLRP3 activation and pyroptosis during Mycobacterium tuberculosis infection. *Nat. Commun.* **11**, 2270 (2020).
14. Bah, A. *et al.* The Lipid Virulence Factors of Mycobacterium tuberculosis Exert Multilayered Control over Autophagy-Related Pathways in Infected Human Macrophages. *Cells* **9**, 666 (2020).
15. Bell, S. L., Lopez, K. L., Cox, J. S., Patrick, K. L. & Watson, R. O. Galectin-8 Senses Phagosomal Damage and Recruits Selective Autophagy Adapter TAX1BP1 To Control Mycobacterium tuberculosis Infection in Macrophages. *mBio* **12**, e01871-20 (2021).
16. Watson, R. O., Manzanillo, P. S. & Cox, J. S. Extracellular M. tuberculosis DNA Targets Bacteria for Autophagy by Activating the Host DNA-Sensing Pathway. *Cell* **150**, 803–815 (2012).
17. Watson, R. O. *et al.* The Cytosolic Sensor cGAS Detects Mycobacterium tuberculosis DNA to Induce Type I Interferons and Activate Autophagy. *Cell Host Microbe* **17**, 811–819 (2015).
18. Franco, L. H. *et al.* The Ubiquitin Ligase Smurf1 Functions in Selective Autophagy of Mycobacterium tuberculosis and Anti-tuberculous Host Defense. *Cell Host Microbe* **21**, 59–72 (2017).
19. Sanjuan, M. A. *et al.* Toll-like receptor signalling in macrophages links the autophagy pathway to phagocytosis. *Nature* **450**, 1253–1257 (2007).
20. Martinez, J. *et al.* Molecular characterization of LC3-associated phagocytosis reveals distinct roles for Rubicon, NOX2 and autophagy proteins. *Nat. Cell Biol.* **17**, 893–906 (2015).
21. Upadhyay, S. & Philips, J. A. LC3-associated phagocytosis: host defense and microbial response. *Curr. Opin. Immunol.* **60**, 81–90 (2019).
22. Cemma, M., Grinstein, S. & Brumell, J. H. Autophagy proteins are not universally required for phagosome maturation. *Autophagy* **12**, 1440–1446 (2016).

23. Cardenal-Muñoz, E. *et al.* Mycobacterium marinum antagonistically induces an autophagic response while repressing the autophagic flux in a TORC1- and ESX-1-dependent manner. *PLOS Pathog.* **13**, e1006344 (2017).
24. López-Jiménez, A. T. *et al.* The ESCRT and autophagy machineries cooperate to repair ESX-1-dependent damage at the Mycobacterium-containing vacuole but have opposite impact on containing the infection. *PLOS Pathog.* **14**, e1007501 (2018).
25. Romagnoli, A. *et al.* ESX-1 dependent impairment of autophagic flux by Mycobacterium tuberculosis in human dendritic cells. *Autophagy* **8**, 1357–1370 (2012).
26. Chandra, P. *et al.* Mycobacterium tuberculosis Inhibits RAB7 Recruitment to Selectively Modulate Autophagy Flux in Macrophages. *Sci. Rep.* **5**, 16320 (2015).
27. Saini, N. K. *et al.* Suppression of autophagy and antigen presentation by Mycobacterium tuberculosis PE_PGRS47. *Nat. Microbiol.* **1**, 1–12 (2016).
28. Shin, D.-M. *et al.* Mycobacterium tuberculosis Eis Regulates Autophagy, Inflammation, and Cell Death through Redox-dependent Signaling. *PLOS Pathog.* **6**, e1001230 (2010).
29. Strong, E. J. *et al.* Identification of Autophagy-Inhibiting Factors of Mycobacterium tuberculosis by High-Throughput Loss-of-Function Screening. *Infect. Immun.* **88**, e00269-20 (2020).
30. Strong, E. J., Ng, T. W., Porcelli, S. A. & Lee, S. Mycobacterium tuberculosis PE_PGRS20 and PE_PGRS47 Proteins Inhibit Autophagy by Interaction with Rab1A. *mSphere* **6**, e00549-21 (2021).
31. Köster, S. *et al. Mycobacterium tuberculosis* is protected from NADPH oxidase and LC3-associated phagocytosis by the LCP protein CpsA. *Proc. Natl. Acad. Sci.* **114**, E8711–E8720 (2017).
32. Kolloli, A. & Subbian, S. Host-Directed Therapeutic Strategies for Tuberculosis. *Front. Med.* **4**, 171 (2017).
33. Srinivasan, L. *et al.* Identification of a Transcription Factor That Regulates Host Cell Exit and Virulence of Mycobacterium tuberculosis. *PLOS Pathog.* **12**, e1005652 (2016).

34. Gao, W. *et al.* Biochemical Isolation and Characterization of the Tubulovesicular LC3-positive Autophagosomal Compartment *. *J. Biol. Chem.* **285**, 1371–1383 (2010).

35. Lerner, T. R. *et al. Mycobacterium tuberculosis* cords within lymphatic endothelial cells to evade host immunity. *JCI Insight* **5**, (2020).

36. Stringer, C. & Pachitariu, M. Cellpose 2.0: how to train your own model. 2022.04.01.486764 Preprint at https://doi.org/10.1101/2022.04.01.486764 (2022).

37. Armstrong, J. A. & Hart, P. D. Phagosome-lysosome interactions in cultured macrophages infected with virulent tubercle bacilli. Reversal of the usual nonfusion pattern and observations on bacterial survival. *J. Exp. Med.* **142**, 1–16 (1975).

38. Sturgill-Koszycki, S. *et al.* Lack of Acidification in Mycobacterium Phagosomes Produced by Exclusion of the Vesicular Proton-ATPase. *Science* **263**, 678–681 (1994).

39. Clemens, D. L. & Horwitz, M. A. Characterization of the Mycobacterium tuberculosis phagosome and evidence that phagosomal maturation is inhibited. *J. Exp. Med.* **181**, 257–270 (1995).

40. Hasan, Z. *et al.* Isolation and characterization of the mycobacterial phagosome: segregation from the endosomal/lysosomal pathway. *Mol. Microbiol.* **24**, 545–553 (1997).

41. Fratti, R. A., Backer, J. M., Gruenberg, J., Corvera, S. & Deretic, V. Role of phosphatidylinositol 3-kinase and Rab5 effectors in phagosomal biogenesis and mycobacterial phagosome maturation arrest. *J. Cell Biol.* **154**, 631–644 (2001).

42. Bach, H., Papavinasasundaram, K. G., Wong, D., Hmama, Z. & Av-Gay, Y. Mycobacterium tuberculosis Virulence Is Mediated by PtpA Dephosphorylation of Human Vacuolar Protein Sorting 33B. *Cell Host Microbe* **3**, 316–322 (2008).

43. van der Wel, N. *et al.* M. tuberculosis and M. leprae Translocate from the Phagolysosome to the Cytosol in Myeloid Cells. *Cell* **129**, 1287–1298 (2007).

44. Simeone, R. *et al.* Phagosomal Rupture by Mycobacterium tuberculosis Results in Toxicity and Host Cell Death. *PLoS Pathog.* **8**, e1002507 (2012).

45. Levitte, S. *et al.* Mycobacterial Acid Tolerance Enables Phagolysosomal Survival and Establishment of Tuberculous Infection In Vivo. *Cell Host Microbe* **20**, 250–258 (2016).

46. Gutierrez, M. G. & Enninga, J. Intracellular niche switching as host subversion strategy of bacterial pathogens. *Curr. Opin. Cell Biol.* **76**, 102081 (2022).

47. Baker, J. J., Johnson, B. K. & Abramovitch, R. B. Slow growth of Mycobacterium tuberculosis at acidic pH is regulated by phoPR and host-associated carbon sources. *Mol. Microbiol.* **94**, 56–69 (2014).

48. Frigui, W. *et al.* Control of M. tuberculosis ESAT-6 Secretion and Specific T Cell Recognition by PhoP. *PLOS Pathog.* **4**, e33 (2008).

49. Ma, Y., Keil, V. & Sun, J. Characterization of *Mycobacterium tuberculosis* EsxA Membrane Insertion: ROLES OF N- AND C-TERMINAL FLEXIBLE ARMS AND CENTRAL HELIX-TURN-HELIX MOTIF. *J. Biol. Chem.* **290**, 7314–7322 (2015).

50. De Leon, J. *et al. Mycobacterium tuberculosis* ESAT-6 Exhibits a Unique Membrane-interacting Activity That Is Not Found in Its Ortholog from Non-pathogenic *Mycobacterium smegmatis*. *J. Biol. Chem.* **287**, 44184–44191 (2012).

51. de Jonge, M. I. *et al.* ESAT-6 from Mycobacterium tuberculosis Dissociates from Its Putative Chaperone CFP-10 under Acidic Conditions and Exhibits Membrane-Lysing Activity. *J. Bacteriol.* **189**, 6028–6034 (2007).

52. Simeone, R. *et al.* Cytosolic Access of Mycobacterium tuberculosis: Critical Impact of Phagosomal Acidification Control and Demonstration of Occurrence In Vivo. *PLOS Pathog.* **11**, e1004650 (2015).

53. Augenstreich, J. *et al.* ESX-1 and phthiocerol dimycocerosates of *Mycobacterium tuberculosis* act in concert to cause phagosomal rupture and host cell apoptosis. *Cell. Microbiol.* **19**, e12726 (2017).

54. Repnik, U. *et al.* L-leucyl-L-leucine methyl ester does not release cysteine cathepsins to the cytosol but inactivates them in transiently permeabilized lysosomes. *J. Cell Sci.* **130**, 3124–3140 (2017).

55. Radulovic, M. *et al.* ESCRT-mediated lysosome repair precedes lysophagy and promotes cell survival. *EMBO J.* **37**, e99753 (2018).

56. Skowyra, M. L., Schlesinger, P. H., Naismith, T. V. & Hanson, P. I. Triggered recruitment of ESCRT machinery promotes endolysosomal repair. *Science* **360**, eaar5078 (2018).

57. Radulovic, M. *et al.* Lysosome repair by ER-mediated cholesterol transfer. 2022.09.26.509457 Preprint at https://doi.org/10.1101/2022.09.26.509457 (2022).

58. Schnettger, L. *et al.* A Rab20-Dependent Membrane Trafficking Pathway Controls M. tuberculosis Replication by Regulating Phagosome Spaciousness and Integrity. *Cell Host Microbe* **21**, 619-628.e5 (2017).

59. Kreibich, S. *et al.* Autophagy Proteins Promote Repair of Endosomal Membranes Damaged by the Salmonella Type Three Secretion System 1. *Cell Host Microbe* **18**, 527–537 (2015).

60. Peña-Martinez, C., Rickman, A. D. & Heckmann, B. L. Beyond autophagy: LC3-associated phagocytosis and endocytosis. *Sci. Adv.* **8**, eabn1702 (2022).

61. Hooper, K. M. *et al.* V-ATPase is a universal regulator of LC3-associated phagocytosis and non-canonical autophagy. *J. Cell Biol.* **221**, e202105112 (2022).

62. Johnsson, K., Froland, W. A. & Schultz, P. G. Overexpression, Purification, and Characterization of the Catalase-peroxidase KatG from Mycobacterium tuberculosis*. *J. Biol. Chem.* **272**, 2834–2840 (1997).

63. Braunstein, M., Espinosa, B. J., Chan, J., Belisle, J. T. & R. Jacobs Jr, W. SecA2 functions in the secretion of superoxide dismutase A and in the virulence of Mycobacterium tuberculosis. *Mol. Microbiol.* **48**, 453–464 (2003).

64. Miller, J. L., Velmurugan, K., Cowan, M. J. & Briken, V. The Type I NADH Dehydrogenase of Mycobacterium tuberculosis Counters Phagosomal NOX2 Activity to Inhibit TNF-α-Mediated Host Cell Apoptosis. *PLOS Pathog.* **6**, e1000864 (2010).

65. Srivastava, S., Battu, M. B., Khan, M. Z., Nandicoori, V. K. & Mukhopadhyay, S. Mycobacterium tuberculosis PPE2 Protein Interacts with p67phox and Inhibits Reactive Oxygen Species Production. *J. Immunol.* **203**, 1218–1229 (2019).

66. Emami, N., Sedaei, Z. & Ferdousi, R. Computerized cell tracking: Current methods, tools and challenges. *Vis. Inform.* **5**, 1–13 (2021).

67. Huth, J. *et al.* Significantly improved precision of cell migration analysis in time-lapse video microscopy through use of a fully automated tracking system. *BMC Cell Biol.* **11**, 24 (2010).

68. Simpson, D. S. *et al.* Interferon-γ primes macrophages for pathogen ligand-induced killing via a caspase-8 and mitochondrial cell death pathway. *Immunity* **55**, 423-441.e9 (2022).

69. Quigley, J. *et al.* The Cell Wall Lipid PDIM Contributes to Phagosomal Escape and Host Cell Exit of Mycobacterium tuberculosis. *mBio* **8**, mBio.00148-17, e00148-17 (2017).

70. Schnettger, L. & Gutierrez, M. G. Quantitative Spatiotemporal Analysis of Phagosome Maturation in Live Cells. in *Phagocytosis and Phagosomes: Methods and Protocols* (ed. Botelho, R.) 169–184 (Springer, 2017). doi:10.1007/978-1-4939-6581-6_11.

Figure 1

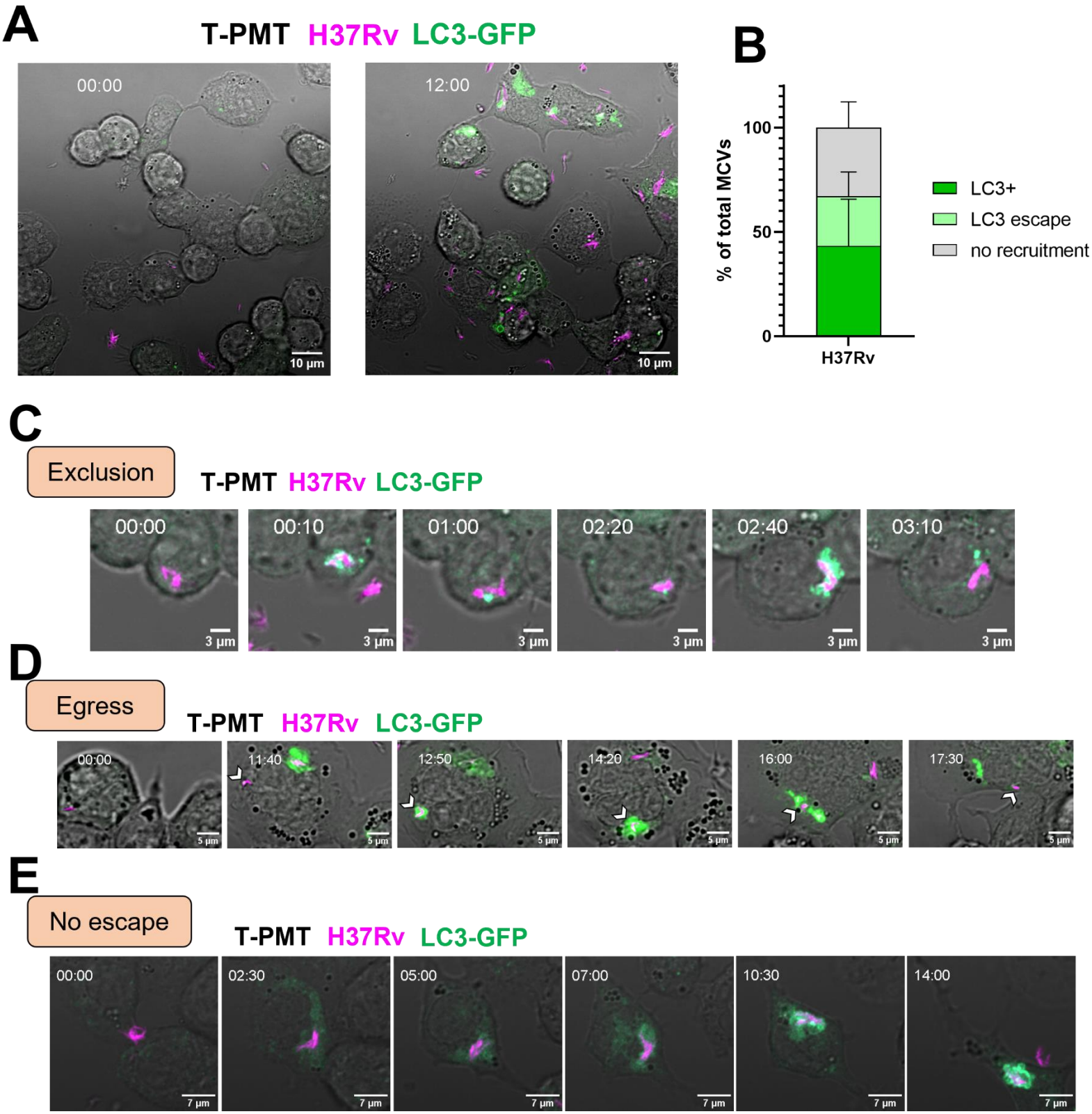
A
T-PMT H37Rv LC3-GFP
00:00
12:00
10 µm
10 µm
B
% of total MCVs
100
50
0
H37Rv
LC3+
LC3 escape
no recruitment
C
Exclusion
T-PMT H37Rv LC3-GFP
00:00
00:10
01:00
02:20
02:40
03:10
3 µm
D
Egress
T-PMT H37Rv LC3-GFP
00:00
11:40
12:50
14:20
16:00
17:30
5 µm
E
No escape
T-PMT H37Rv LC3-GFP
00:00
02:30
05:00
07:00
10:30
14:00
7 µm

Figure 2

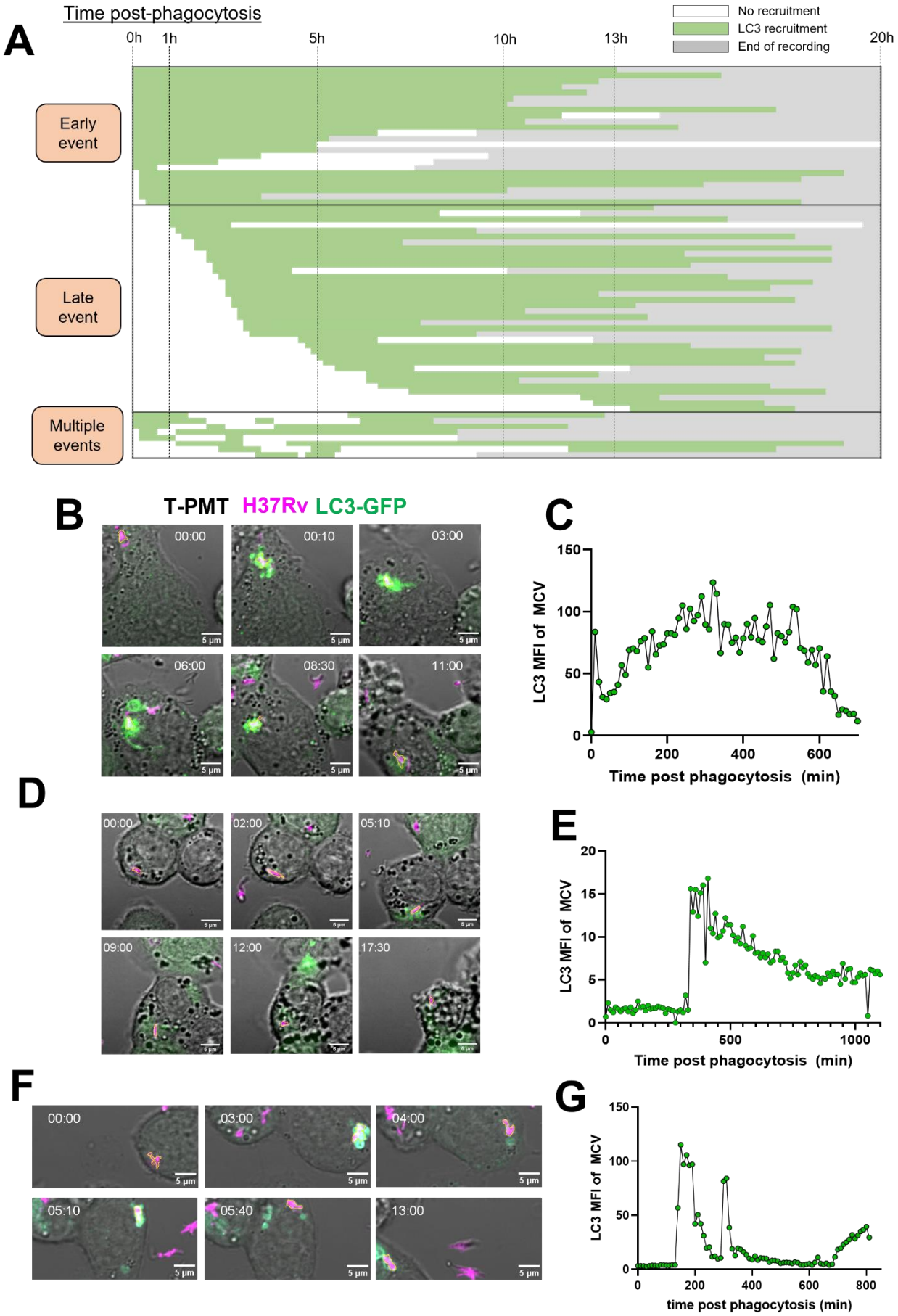
A
Time post-phagocytosis
0h
1h
5h
10h
13h
20h
No recruitment
LC3 recruitment
End of recording
Early event
Late event
Multiple events
B
T-PMT H37Rv LC3-GFP
00:00
00:10
03:00
06:00
08:30
11:00
5 µm
C
LC3 MFI of MCV
Time post phagocytosis (min)
D
00:00
02:00
05:10
09:00
12:00
17:30
E
LC3 MFI of MCV
Time post phagocytosis (min)
F
00:00
03:00
04:00
05:10
05:40
13:00
G
LC3 MFI of MCV
time post phagocytosis (min)

Figure 3

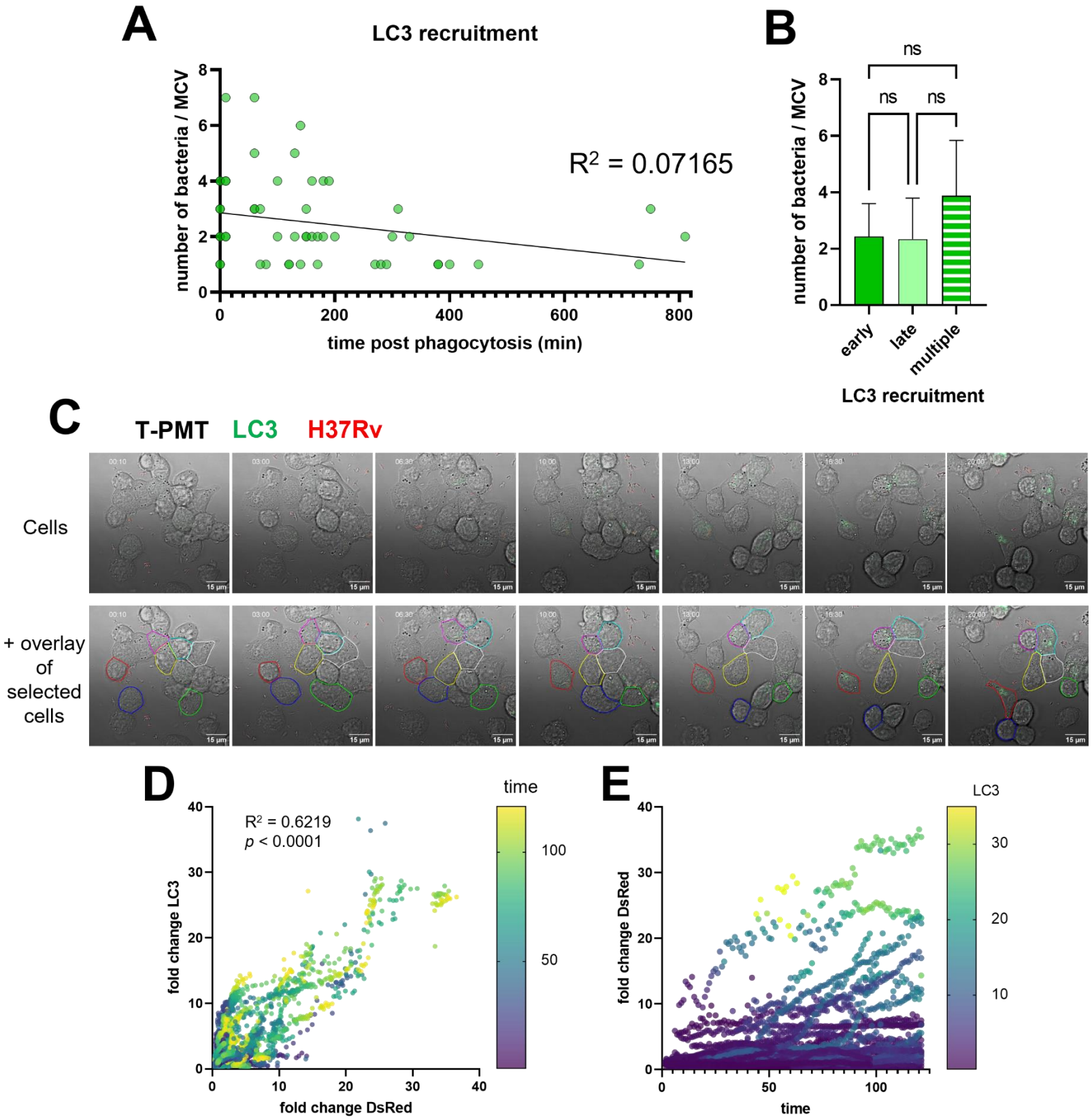
A
LC3 recruitment
number of bacteria / MCV
time post phagocytosis (min)
R² = 0.07165
B
ns
ns
ns
number of bacteria / MCV
early
late
multiple
LC3 recruitment
C
T-PMT
LC3
H37Rv
Cells
+ overlay of selected cells
D
R² = 0.6219
p < 0.0001
fold change LC3
fold change DsRed
time
E
fold change DsRed
time
LC3

Figure 4

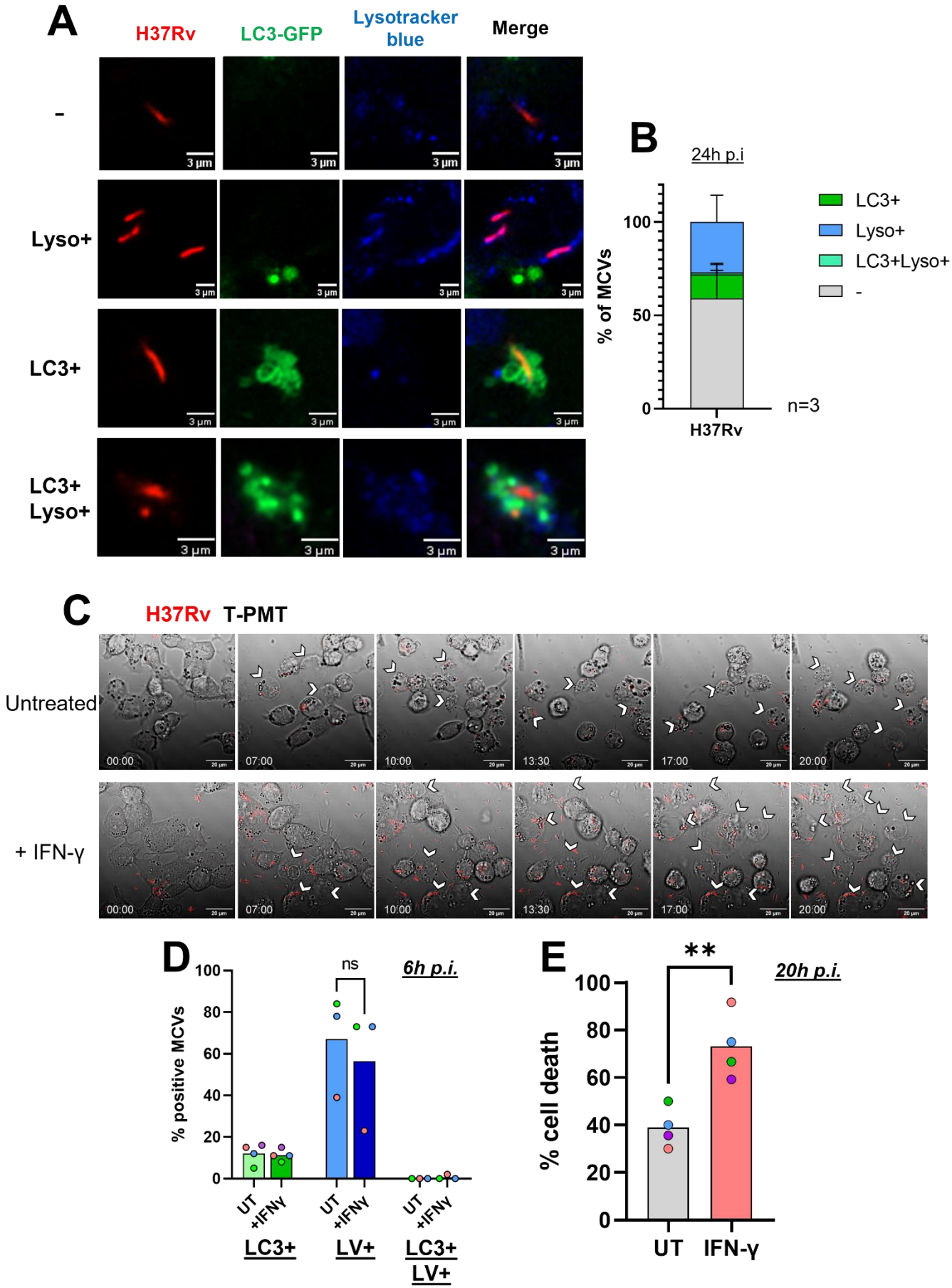
A
H37Rv
LC3-GFP
Lysotracker blue
Merge
-
Lyso+
LC3+
LC3+ Lyso+
3 µm
B
24h p.i
% of MCVs
100
50
0
H37Rv
n=3
LC3+
Lyso+
LC3+Lyso+
-
C
H37Rv T-PMT
Untreated
+ IFN-γ
00:00
07:00
10:00
13:30
17:00
20:00
D
% positive MCVs
ns
6h p.i.
UT
+IFNγ
LC3+
LV+
LC3+ LV+
E
**
20h p.i.
% cell death
UT
IFN-γ

Figure 5

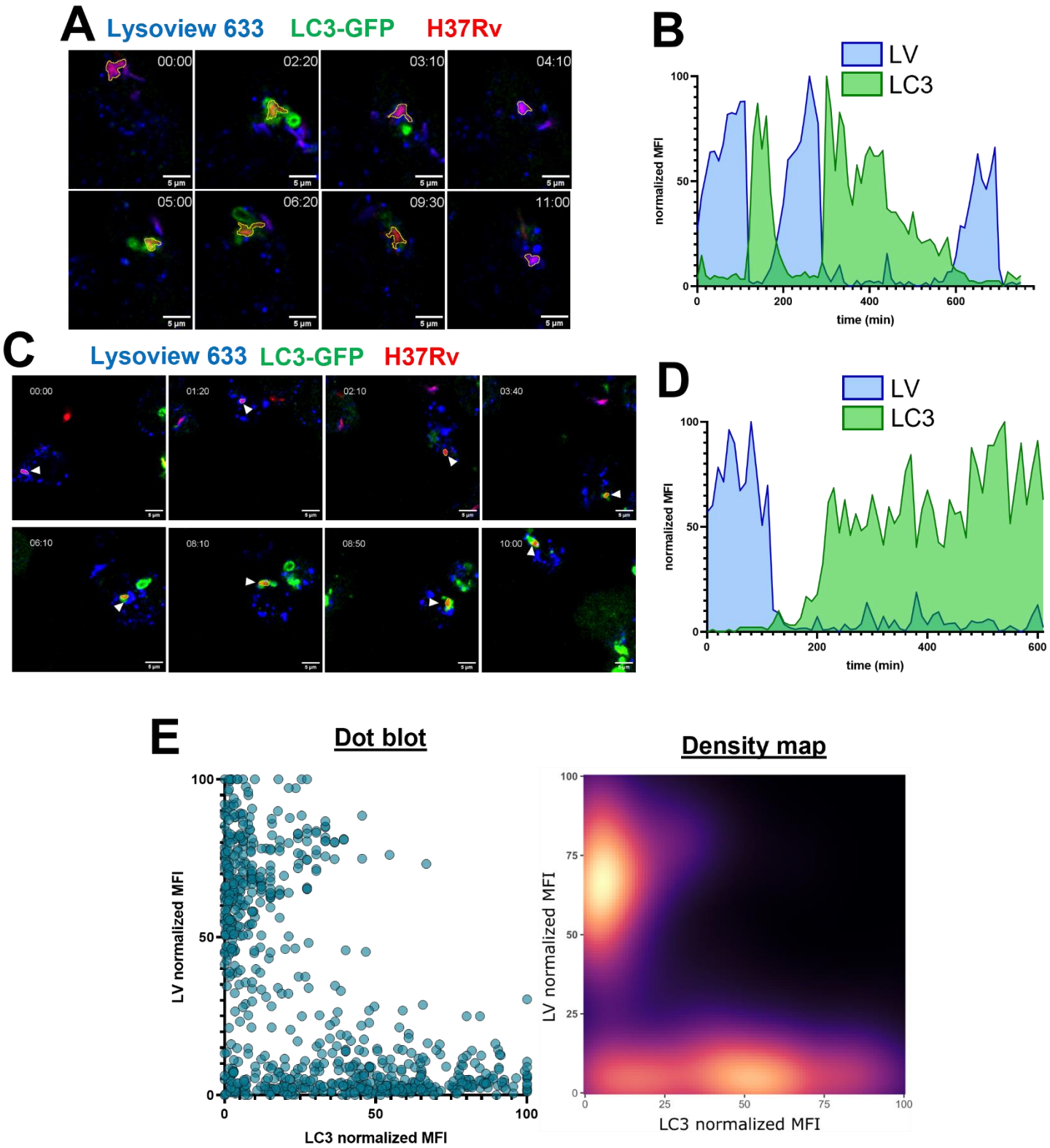
A
Lysoview 633
LC3-GFP
H37Rv
00:00
02:20
03:10
04:10
05:00
06:20
09:30
11:00
5 µm
B
LV
LC3
normalized MFI
time (min)
C
Lysoview 633
LC3-GFP
H37Rv
00:00
01:20
02:10
03:40
06:10
08:10
08:50
10:00
D
LV
LC3
normalized MFI
time (min)
E
Dot blot
LV normalized MFI
LC3 normalized MFI
Density map
LV normalized MFI
LC3 normalized MFI

Figure 6

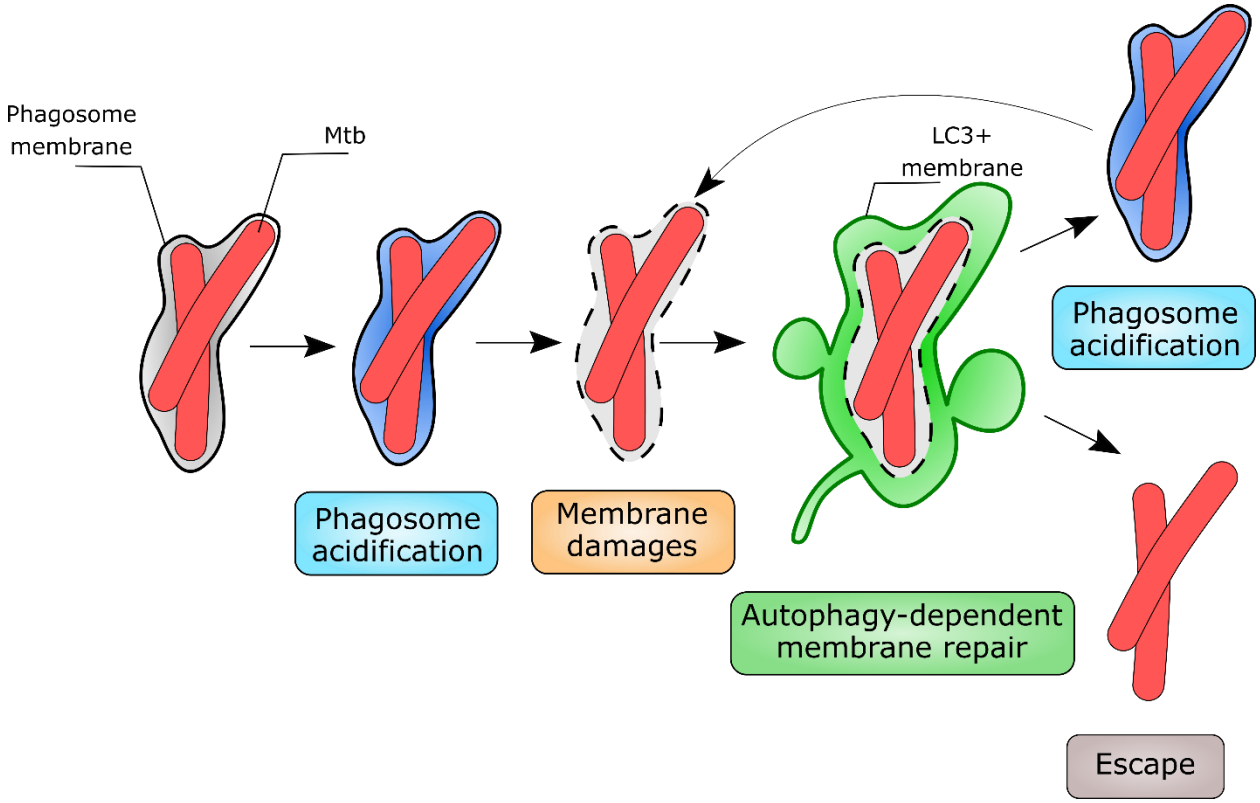
Phagosome membrane
Mtb
LC3+ membrane
Phagosome acidification
Phagosome acidification
Membrane damages
Autophagy-dependent membrane repair
Escape

Figure S1

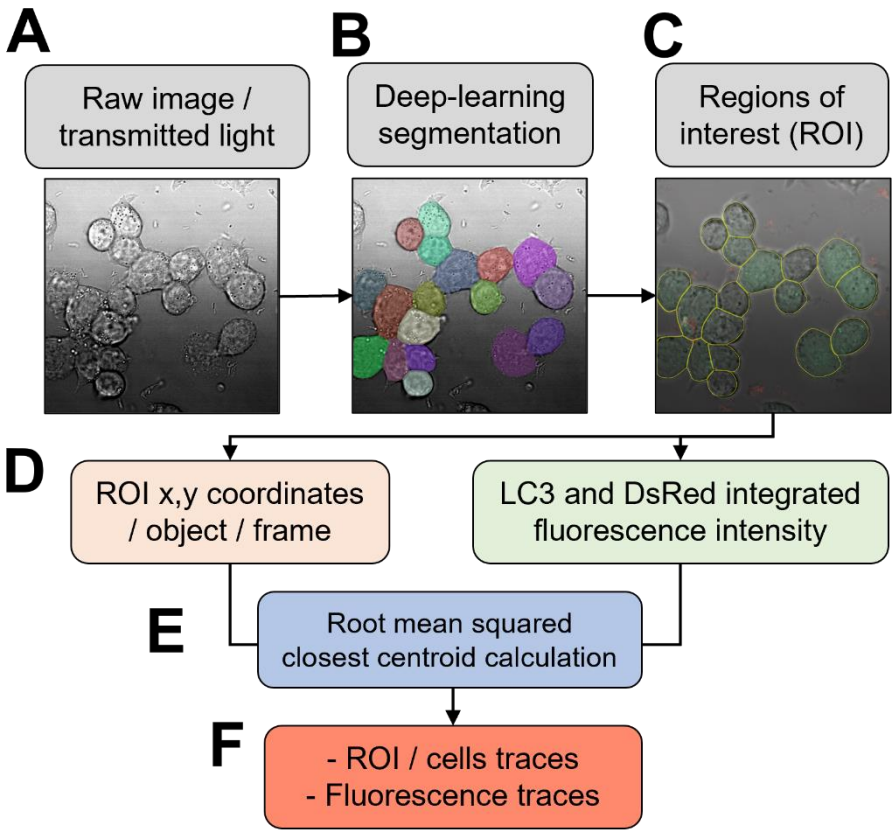
A
Raw image / transmitted light
B
Deep-learning segmentation
C
Regions of interest (ROI)
D
ROI x,y coordinates / object / frame
LC3 and DsRed integrated fluorescence intensity
E
Root mean squared closest centroid calculation
F
- ROI / cells traces
- Fluorescence traces

Figure S2

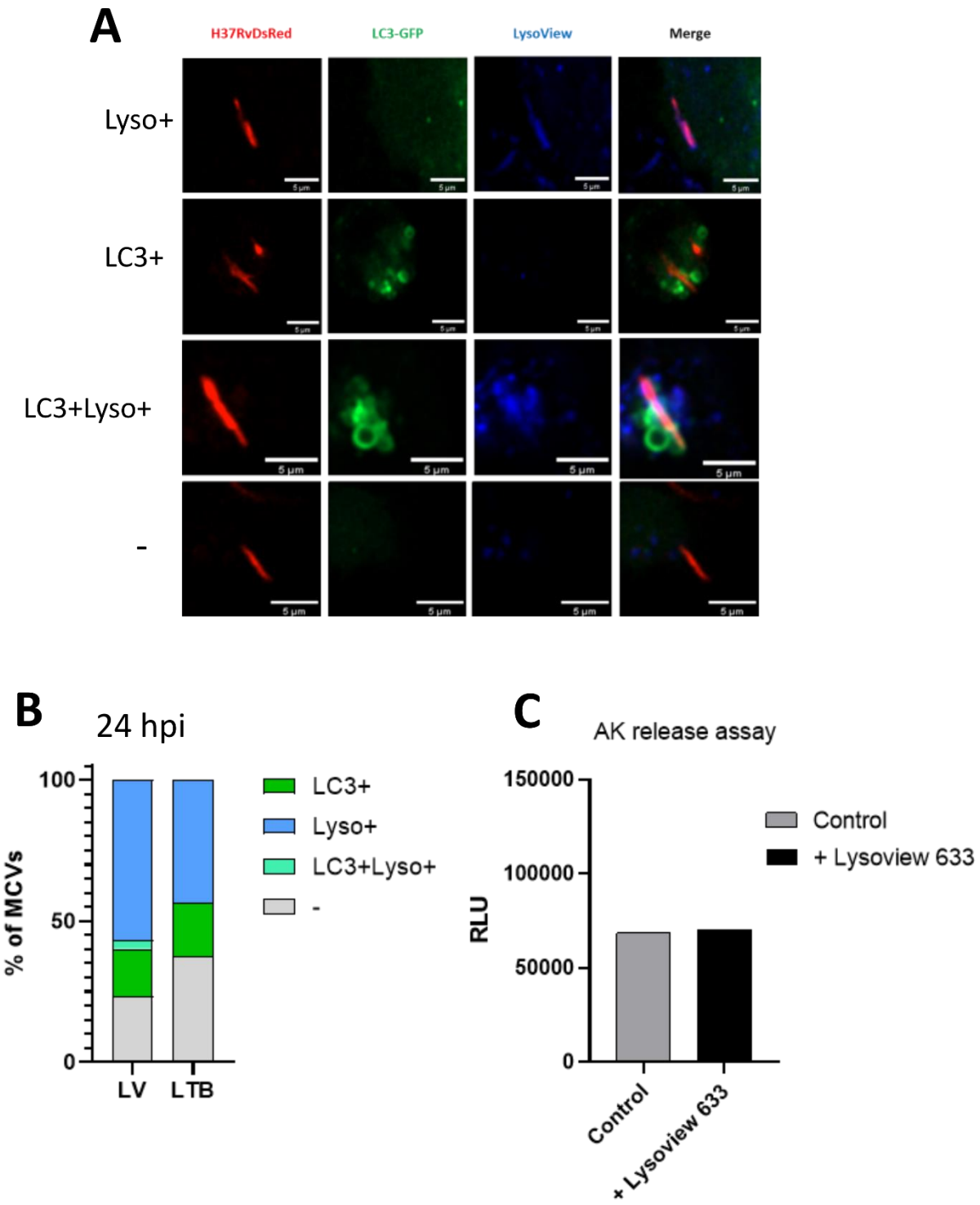
A
H37RvDsRed
LC3-GFP
LysoView
Merge
Lyso+
LC3+
LC3+Lyso+
-
5 µm
B
24 hpi
% of MCVs
100
50
0
LV
LTB
LC3+
Lyso+
LC3+Lyso+
-
C
AK release assay
RLU
150000
100000
50000
0
Control
+ Lysoview 633
Control
+ Lysoview 633

Figure S3

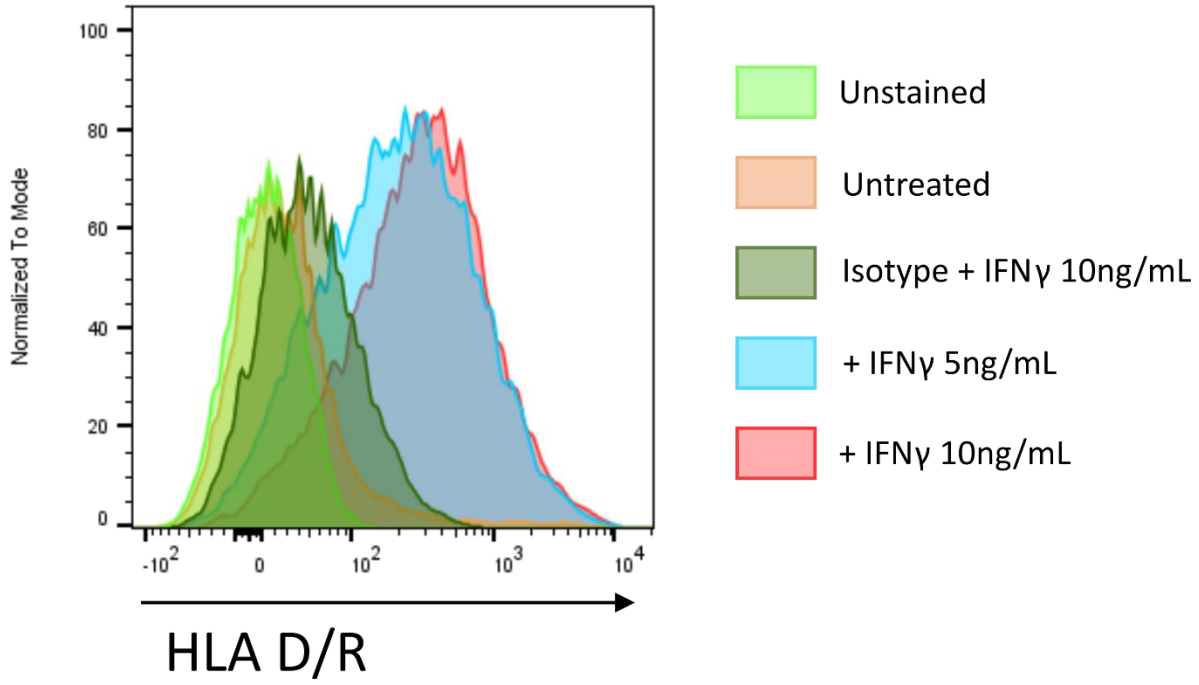

Figure S4

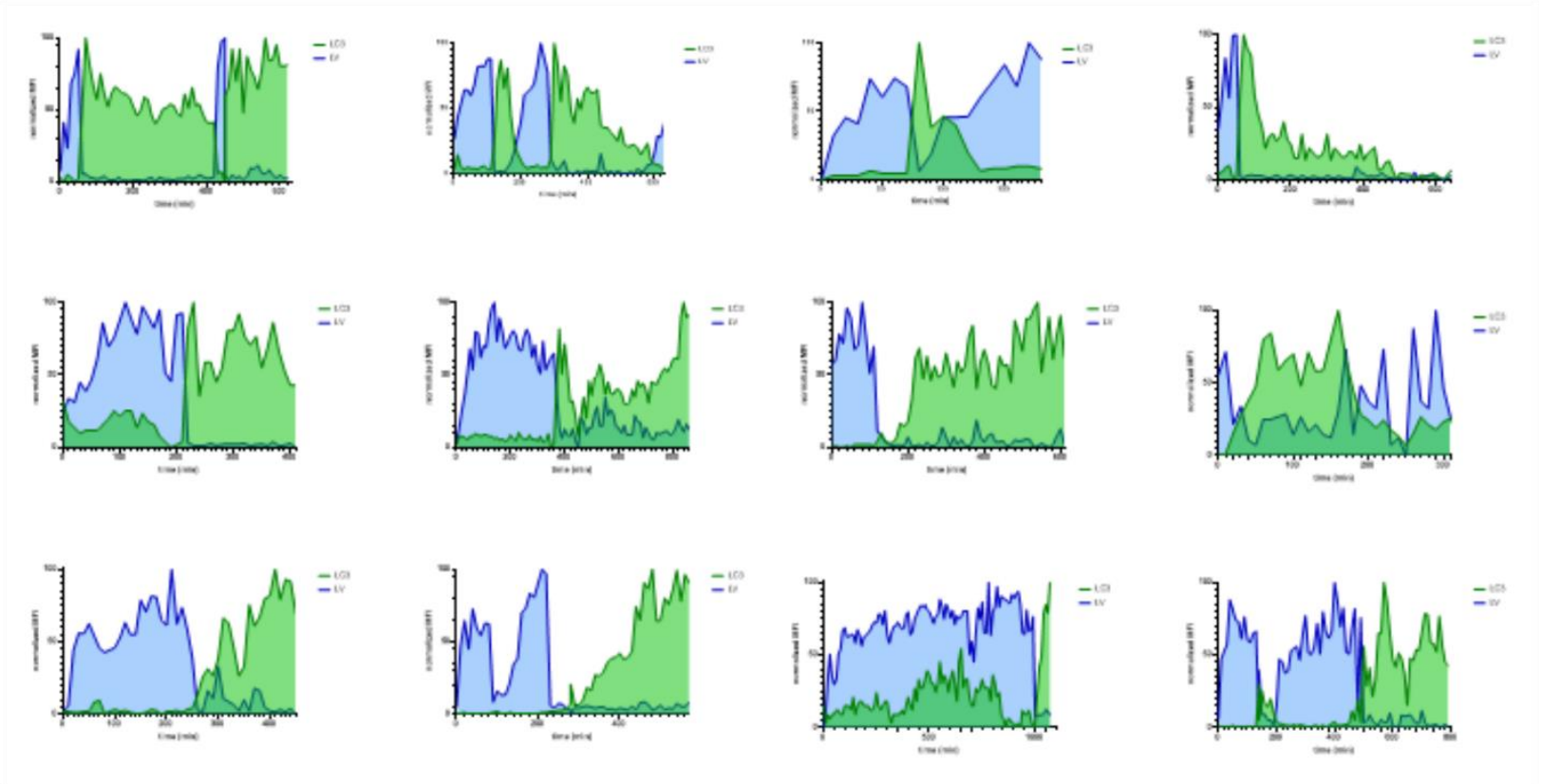

Figure legends

Figure 1: The Mtb phagosome induces frequent LC3 recruitment but can escape from it.
THP-1 cells stably expressing LC3-GFP were infected with DsRed-expressing MtbH37Rv at an MOI of 2 for a course of 16 – 20h. A 9µm z-stack with a 1µm step was recorded every 10 minutes. (A) A representative image of infected THP-1 cells at the beginning of recording and at 12h post-infection. Time stamp format is hh:mm. (B) quantification of LC3 recruitment to mycobacteria-containing vacuoles (MCVs) ($LC3^+$), and subsequent LC3 escape or no LC3 recruitment. The graph shows the mean and standard deviation from 4 independent experiments. (C) Representative time lapse images extracted from movie 2 of LC3 recruitment to an MCV followed by loss of LC3 signal by exclusion. (D) Representative time lapse images extracted from movie 3 of LC3 recruitment to an MCV followed signal by egress of the bacteria out of the autophagosome. (E) Representative time lapse of an MCV exhibiting a LC3 recruitment

Figure 2: LC3 recruitment does not follow a specific timing pattern
(A) MCVs were categorized by their time of observed LC3 recruitment after phagocytosis. The green color indicates visually observed LC3 recruitment, and the white color no recruitment. The grey color indicates end of recording. The total number of MCVs observed was n=73. MCVs were organized into 3 categories: 1. "Early events" the ones showing LC3 recruitment immediately or shortly after phagocytosis (≤1h post phagocytosis), 2. "Late events" the MCVs showing an LC3 recruitment > 1h post phagocytosis and 3. "multiple events" the MCVs showing multiple LC3 recruitments. (B,D,F) Representative time lapses of MCVs of the 3 listed categories, extracted from movie 4, 5 and 6 respectively. MCVs followed were outlines with a yellow region of interest (ROI) line. (C,E,G) Confirmation of visual recruitment by quantification of LC3 fluorescence intensity over time on the three MCVs in (B,D,F).

Figure 3: Macrophages bacterial burden is the main driver for LC3 recruitment to MCVs
(A) Distribution of number of bacteria per MCVs compared to the time of observed of LC3 recruitment. (B) Quantification of the average number of bacteria per MCV in each group from figure 2A. (n=29 early event, n=36 late event and n=8 multiple events). The groups were compared by one-way ANOVA test followed by Dunnett *post-hoc* statistical test. (C) Representative time lapse with or without overlay showing the result of the single cell tracking and quantification described in methodology. (D+E) Single cell tracking and quantification of GFP (LC3) and DsRed (H37Rv) fluorescence intensity over time plotted on a 3 variables graph. Each dot represents 1 cell at 1 frame. Data are shown in fold change from MFI at frame 1. Left panel, Pearson r correlation coefficient was calculated between LC3 and DsRed fluorescence values. n = 3595 from 31 cells, R^2 and *p* value are displayed on graph.

Figure 4: Autophagosomes are not bactericidal and IFN-γ treatment has no effect on LC3 recruitment frequency or phagosome maturation
(A-B) THP-1 expressing LC3-GFP were infected at an MOI of 10 for 4h and incubated for 24h. Cells were then stained for Lysotracker blue and imaged by confocal microscopy. (A) representative image of MCVs that were unstained, positive for LC3 alone (LC3+), positive for lysotracker alone (Lyso+), or double positive (LC3+Lyso+). (B) quantification of LC3 and Lysotracker staining on MCVs. The data were obtained from 3 independent experiments. (C-E) THP-1-LC3-GFP cells were treated with IFN-γ 10ng/mL or left untreated overnight and infected with DsRed expressing H37Rv at MOI 2. Cells were also stained with Lysoview-633 (LV) and the dye was kept during image acquisition. Cells were image by time lapse confocal microscopy. (C) Representative time lapse showing the untreated cells (top panel) or pre-stimulated with IFN-γ (bottom panel). Time stamp format is hh:mm. Chevrons are showing cells presenting the ballooning phenotype. (D) Quantification of LC3 and/or Lysoview association to MCVs. Data are from 3 to 4 independent experiments. The color of the points indicates data obtained from the same experiment.

Data between untreated and IFN-γ treated cells were compared by unpaired *t*-test. ns = non-significant. (E) Quantification of cell death by counting of the proportion of cells exhibiting the ballooning phenotype during infection. Data are from 4 independent experiments. Points' color is representative of the same experiment. Data between untreated and IFN-γ treated groups were compared by unpaired *t*-test. $**p < 0.01$

Figure 5: LC3 recruitment and phagosome maturation are mutually exclusive
Single MCV tracking in unstimulated THP-1-LC3-GFP cells infected with DsRed expressing H37Rv in figure 4. (A, C) representative time lapses of MCVs outlined with a yellow ROI. (B, D) quantification of fluorescence at the MCV for each time point. Mean fluorescence intensity of GFP and Lysoview was measured and normalized between values of 0 and 100 as 0 the minimum value recorded, and 100 the maximum value. (E, left panel) Quantification of Lysoview and LC3 normalized MFI and was compared. Each dot represents the GFP and LV normalized MFI at one time point for one MCV from 3 independent experiments (n=12 MCVs). The individual fluorescence traces of each MCVs are shown in Figure S4. (E, right panel) The distribution of data points in left panel is shown as a density map.

Figure 6: Model of LC3 recruitment to the Mtb phagosome
After phagocytosis, the MCV may undergo acidification. This acidification is lost upon induction of membrane damage which triggers LC3 recruitment. This autophagy-related membrane repair response eventually allows the rescue of acidification of the phagosome, that can be later damaged again. The bacterium is eventually able to physically escape from the phagosome or the LC3 positive vacuole to reside in the cytosol.

Figure S1: Diagram of the image analysis workflow used for the quantitative single cell tracking
(A) A single slice in the transmitted light (T-PMT) channel was first isolated on imageJ using the function "make substack". (B) The cells in each time frame were segmented using the Cellpose 2.0 sofware[1]. (C) the segmentation mask obtained was used to generate ROIs around the cells by the "edge detection function" on ImageJ. (D) The ROIs were used to obtain their respective object ID, x,y coordinate, frame number, and the associated integrated fluorescence intensity of LC3 and DsRed. (E) ROIs / Cells were linked from one frame to the next by root mean squared closest centroid calculation. (F) ROIs traces were reconstructed and allowed to reconstruct the fluorescence traces from the data obtained in (D).

Figure S2: Comparison between Lysoview-633 and Lysotracker blue staining on infected cells
(A) Representative images of MCVs in THP-1-LC3-GFP cells negative (-), positive for Lysoview 633 (Lyso+), for LC3 (LC3+), and double positive (LC3+Lyso+). (B) quantification of the fraction of MCVs in THP-1 cells stained for lysoview 633 or lysotracker blue. (C) The cell death level was quantified by the adenylate Kinase (AK) release assay on THP-1-LC3-GFP treated or not with Lysoview 633 1:2000 for 48h. RLU = relative luminescence unit

Figure S3: Effect of IFN-γ stimulation on MHC-II expression.
THP-1 cells were treated with IFN-γ 5ng/mL, 10ng/mL overnight or left untreated. Cells were fixed and stained for MHC-II expression using HLA/DR antibody (BD). Some Treated cells with 10ng/mL were stained with isotype control. The staining was analyzed by flow cytometry.

Figure S4 : Fluorescence traces of LC3 and lysoview of individual MCVs
Compilation of the LC3 and lysoview fluorescence quantification on individual MCVs isolated from 4 independent experiments. Only the MCV exhibiting LC3 recruitment for more than 3h were retained.

Movie legends

Movie 1: Representative field of view from a time lapse experiment monitoring LC3 recruitment to MCVs.
THP-1 cells expressing LC3-GFP (green) were infected with H37Rv-DsRed (red) at an MOI 2 and imaged for 20h. A 10µm z-stack was acquired every 10 minutes. Time stamp format is hh:mm, and only one slice is shown. Example images are shown in Figure 1A.

Movie 2: Representative time lapse of LC3 recruitment to the MCV followed by the exclusion of LC3 signal.
A THP-1 cell expressing LC3-GFP (green) infected with H37Rv-DsRed (red) is shown. Time stamp format is hh:mm. Time 00:00 is the frame in which the bacteria visually enter the cell. Example images are shown in Figure 1C.

Movie 3: Representative time lapse of LC3 recruitment to the MCV followed by the egress of the bacteria away from the LC3 vesicles.
A THP-1 cell expressing LC3-GFP (green) infected with H37Rv-DsRed (red) is shown. Time stamp format is hh:mm. Time 00:00 is the frame in which the bacteria visually enter the cell. Example images are shown in Figure 1D.

Movie 4: Representative time lapse of a LC3 recruitment to the MCV without sign of escape from the bacteria.
A THP-1 cell expressing LC3-GFP (green) infected with H37Rv-DsRed (red) is shown. Time stamp format is hh:mm. Time 00:00 is the frame in which the bacteria visually enter the cell. Example images are shown in Figure 1E.

Movie 5: Representative time lapse of an early LC3 recruitment to the MCV.
A THP-1 cell expressing LC3-GFP (green) infected with H37Rv-DsRed (red) is shown. Time stamp format is hh:mm. Time 00:00 is the frame in which the bacteria visually enter the cell. The yellow outline is an ROI generated for the tracking of the MCV and fluorescence quantification. Example images are shown in Figure 2B.

Movie 6: Representative time lapse of a late LC3 recruitment to the MCV.
A THP-1 cell expressing LC3-GFP (green) infected with H37Rv-DsRed (red) is shown. Time stamp format is hh:mm. Time 00:00 is the frame in which the bacteria visually enter the cell. The yellow outline is an ROI generated for the tracking of the MCV and fluorescence quantification. Example images are shown in Figure 2D.

Movie 7: Representative time lapse of multiple LC3 recruitments to the MCV.
A THP-1 cell expressing LC3-GFP (green) infected with H37Rv-DsRed (red) is shown. Time stamp format is hh:mm. Time 00:00 is the frame in which the bacteria visually enter the cell. The yellow outline is an ROI generated for the tracking of the MCV and fluorescence quantification. Example images are shown in Figure 2F.

Movie 8: Representative field of view from a time lapse experiment showing the specific tracking of cells that get infected and exhibit LC3 recruitment to the MCV.

THP-1 cells expressing LC3-GFP (green) were infected with H37Rv-DsRed (red) at an MOI 2 and imaged for 20h. A 10µm z-stack was acquired every 10 minutes. Time stamp format is hh:mm, and only one slice is shown. Example images with or without the overlay are shown in Figure 3C.

Movie 9: Representative field of view from a time lapse experiment showing the infection with Mtb of unstimulated cells with Mtb.
THP-1 cells expressing LC3-GFP were infected with H37Rv-DsRed (red) at an MOI 2 and imaged for 20h. A 10µm z-stack was acquired every 10 minutes. Time stamp format is hh:mm, and only one slice is shown. Example images with or without the overlay are shown in Figure 4C top panel.

Movie 10: Representative field of view from a time lapse experiment showing the infection with Mtb of cells pre-stimulated with IFN-γ.
THP-1 cells expressing LC3-GFP were infected with H37Rv-DsRed (red) at an MOI 2 and imaged for 20h. A 10µm z-stack was acquired every 10 minutes. Time stamp format is hh:mm, and only one slice is shown. Example images with or without the overlay are shown in Figure 4C bottom panel.

Movie 11: Representative time lapse of showing the staining of an MCV with lysoview or LC3 recruitment
A THP-1 cell expressing LC3-GFP (green) stained with lysoview-633 (Blue) infected with H37Rv-DsRed (red) is shown. Time stamp format is hh:mm. Time 00:00 is the frame in which the bacteria visually enter the cell. The yellow outline is an ROI generated for the tracking of the MCV and fluorescence quantification. Example images are shown in Figure 5A.

Movie 12: Representative time lapse of showing the staining of an MCV with lysoview or LC3 recruitment
A THP-1 cell expressing LC3-GFP (green) stained with lysoview-633 (Blue) infected with H37Rv-DsRed (red) is shown. Time stamp format is hh:mm. Time 00:00 is the frame in which the bacteria visually enter the cell. The yellow outline is an ROI generated for the tracking of the MCV and fluorescence quantification. Example images are shown in Figure 5B.